Interactions between crack growth and strain-induced transformation

W. W. GERBERICH, P. L. HEMMINGS, Prof V. F. ZACKAY, and Prof E. R. PARKER

Inorganic Materials Research Division, Lawrence Radiation Laboratory, Department of Mineral Technology, College of Engineering, University of California, Berkeley, California.

Summary

The strain-induced austenite to martensite transformation may be used in a controlled way to design ultra-high strength steels. In the present study, such steels had yield strengths greater than 200,000 psi with elongations on the order of 40 percent. The objective was to determine the influence of the strain-induced transformation on crack propagation characteristics in these steels. First, the detailed crack path was followed fractographically. It is shown that cracking first occurs in the martensite followed by tearing in the austenite, the latter occurring in a direction perpendicular to macroscopic crack growth. The result is cracking in a flat mode, even at stress intensity factors near 300 Ksi-in$^{1/2}$.

To make a better material, one would like to preserve strength while increasing the rate of change of energy absorption in the presence of a crack. The strain-induced transformation is such a mechanism to accomplish this. A theoretical model has led to the tentative conclusion that this mechanism may be a greater energy dissipator than other deformation processes and data show K_{Ic} to be as large as 130 Ksi-in$^{1/2}$ and K_c to be as large as 300 Ksi-in$^{1/2}$ at 196° C.

Introduction

The phenomena of strain-induced transformations are not new. They have long been observed in steels, e.g. Hadfield's manganese steel. What is new is the deliberate use of the strain-induced martensitic transformation to prevent necking under tension. Utilizing this philosophy, [1] TRIP steels (*TR*ansformation *I*nduced *P*lasticity) have provided ultimate strengths of 187 Ksi to 312 Ksi with elongations of 75 to 22 percent, respectively. TRIP steels and other steels exhibiting a strain-induced transformation, such as some austenitic stainless steels, generally differ in one or two ways. First, the TRIP steels are chemically balanced so that the M_D is slightly above or at room temperature while the M_S is well below room temperature. Secondly, the austenite is very strong, with yield strengths as great as 240 Ksi. This strength is produced by a combination of precipitation and dislocation multiplication induced by warm working in the range of 250-450 °C. Further, details have been provided by Zackay, *et al.* [1].

What prompted the present investigation was that some unusual crack propagation characteristics were observed in this steel [2]. First, there was a change in fracture mode for thin, very tough specimens that was dependent upon testing speed. The crack growth was either in a flat mode or it abruptly changed to a shear mode after an unusually large amount of slow growth in a flat mode. Secondly, the material was unusually tough even at –196 °C, where plane strain fracture toughness was about 130 Ksi-in$^{1/2}$ for a steel with a yield strength of 230 Ksi. The question immediately arose – can the unusual fracture mode and good toughness be explained in terms of the strain-induced transformation? Two basic alloy compositions, one with an M_D near 20 °C and the other one near 150 °C, were investigated. This provided one material with, and the other one without, the transformation phenomena at room temperature while both exhibited it at –196 °C.

Materials and procedures

With respect to M_D, there were two alloy types of the three alloys investigated. A tabulation of compositions follows:

Heat	C	Cr	Ni	Mo	Si	Mn
A	0·26	10·1	8·8	5·5	2·0	1·7
A'	0·27	9·0	8·0	4·0	2·0	2·0
B	0·20	13·5	8·8	2·9	2·0	2·0

The standard heat treatment was to austenitize at 1200 °C for two hours, brine quench, reheat and deform the austenite 75-80 percent at either 250 °C or 450 °C. As the only variable was austenite deformation temperature, these two treatments will subsequently be referred to as 250 and 450. Tensile samples were normally taken from 0·080 in thick sheet, although some rounds were evaluated from ½ in thick plate. As long as there was a strain-induced transformation, a yield point was observed and is reported as the yield strength. For those few cases where the test did not exhibit a yield point, the 0·2 percent offset yield is reported.

Several types of fracture tests were utilized. Because of material availability, initial plane stress fracture characteristics of thin sheet were evaluated with 3 in by 12 in single-edge notch (SEN) specimens [2]. However, as larger sheet became available, it was desirable to make a more conventional measure of toughness with center-cracked 6 in by 16 in long specimens. Thick plates were evaluated with crack-line loaded samples of the type suggested by Mostovoy, *et al.* [3]. In general, the half-height (H) of the specimen was 1·1 in, the width (W) 2·2 ins,the crack length (a) 0·5 in and the thickness (t) 0·5 in. All specimens were fatigue pre-cracked by extending the crack in about 10,000 cycles of tension-

tension fatigue. Test procedures were those recommended by the ASTM [4, 5] with a calibrated crack-opening displacement gage used to measure crack extension in the thick plates. One deviation was made in the case of the thin sheet in which a few initial tests were run with ink inserted in the notch to follow slow crack growth. It was found that when the crack changed its macroscopic fracture mode from flat to shear, that the ink stopped following. Thus, in subsequent tests the ink was not used and the fracture mode transition was used to mark the end of slow crack growth. It is emphasized that this is an unusual circumstance that should not be generalized.

Stress intensity calculations were made from the collocation results of Srawley, Gross and Brown [5, 6] for both SEN and crack-line loaded configurations. In the case of the center-cracked samples, a secant correction for finite width was preferred to the more familiar tangent correction since it has been shown [7] to give results more closely in line with Isida's [8] analysis. The stress intensity is given by

$$K = \sigma \left[\pi a \sec \frac{\pi a}{W} \right]^{1/2} \tag{1}$$

where σ is the applied stress, a is the half-crack length and W is the specimen width.

Tensile and fracture characteristics

Results of tensile tests are shown in Table 1. All samples except alloy B tested at room temperature exhibited a strain-induced transformation. This resulted in elongations of 18 to 47 percent with ultimate strengths ranging from 222 to 367 Ksi. It is interesting that the yield strength of alloy A' did not increase with decreasing test temperature while the yield strength of alloy B did. In all cases there was a large effect of test temperature on ultimate strength which is a reflection of the large thermal component of yield stress in martensite.

Stress intensity values are enumerated in Tables 2 and 3. With respect to the thin-sheet data, two points are of significance. First, there was an effect of crosshead rate on tests evaluated at room temperature. This is shown in Fig. 1 for alloy A where the toughness increased from 199 to 289 Ksi-in$^{1/2}$ with a two-order magnitude decrease in crosshead rate. It is significant that at the lowest crosshead rate, an instability stress intensity value could not be measured since slow crack growth occurred all the way across the specimen width. This was verified by using ink to follow the growing crack. Significantly, alloy B did not exhibit a similar trend when tested at –196 °C. This will be considered in a subsequent section. Secondly, the toughness level was very high considering

that no plastic zone size corrections were made. This is particularly true at −196 °C where a K/σ_{ys} value of 1·1 is very unusual in steel having an ultimate strength of 327 Ksi at that temperature.

As pertains to the thick plate tests, there was some difficulty in obtaining valid K_{Ic} results. In general, the ½ in thick specimens yielded before any slow crack growth took place. This made it impossible to associate the K values obtained with a plane strain instability. For comparison purposes, three K values were generally measured – one at the deviation in linearity of the load-displacement curve; one using the initial crack length and maximum load and one using the crack length at maximum load with the maximum load. The first two tend to bound K_{Ic} while the latter gives an estimate of the critcial stress intensity for plate of a particular thickness. In general, the toughness results are nearly equal to or greater than 100 Ksi-in$^{1/2}$. One very intriguing point is that there was no thickness transition even up to one-inch thick plate for alloy A' – 450 tested at room temperature. Observations during the test indicated that, even for this thickness, the crack would slowly tear and not propagate rapidly.

An overall observation of the toughness is that it is very good at room temperature and exceptionally good for the ultimate strengths involved at −196 °C. For example, even body-centered cubic martensite such as that found in maraging steel [5] does not have plane strain fracture toughness values greater than 100 Ksi-in$^{1/2}$ for similar strength levels.

Thus, it was not originally anticipated that this material would have exceptional toughness when tested at temperatures where a large volume fraction of body-centered tetragonal martensite would be produced. In the course of these tests, two additional points of significance were noted:

(1) There was a fracture mode transition wherein at a certain point during the crack propagation process there was an abrupt transition from completely flat to completely shear fracture in the case of plane stress. Under plane strain conditions, the transition was from a flat, internally-delaminated fracture to a flat, smooth fracture. These transitions are macroscopically shown in Fig. 2. It should be emphasized that these transitions are not those typically associated with a geometrical effect.

(2) The plastic zone was clearly outlined by the surface tilts due to the strain-induced martensite. For example, a centrally-notched sheet loaded to a stress intensity factor of 191 Ksi-in$^{1/2}$ produced the plastic zone shown in Fig. 3. This allowed estimates of the plastic zone size to be made and led to an interpretation of the various energy absorbing mechanisms involved in the fracture of these steels.

These two points prompted the following hypotheses concerning the role of a strain-induced transformation in the fracture process.

Fracture mode transition

It is first desirable to demonstrate what kind of microscopic fracture mode changes there might be, e.g. cleavage or microvoid coalescence. Fractographically, it was found that crack growth was a microscopically ductile fracture process both before and after the transition. For example, a fractograph taken from the flat, smooth region of a thick sample fractured at −196 °C is shown in Fig. 4. Both wavy slip (center) and dimpled rupture (upper left) regions are noted. Similar microscopic fracture modes were observed before the transition although there was a greater predominance of wavy slip. The wavy slip region is thought to be a type of serpentine glide which is a restricted-flow fracture process. This wavy slip was also observed on the fracture surfaces of alloy A' tested at room temperature.

Additional fractographic evidence of a ductile fracture process was obtained from examining the stretched regions in front of the fatigue precrack. For example, Fig. 5 shows from bottom to top: fatigue striations, a relatively flat region and a wavy slip region. This flat region has been associated with plastic stretching of the crack opening just before the onset of slow crack growth [9]. In Fig. 5, it is seen to be about 2-4 μ in width. One further observation is that stretched regions also resulted along the boundaries of the wavy slip regions. A typical area is shown in Fig. 6. The stretched regions here are also about 2-4 μ in width and thus are comparable in size to those observed in front of the fatigue crack. It is hypothesized that the wavy slip fracture is in the martensitic phase, and proceeds prior to failure in the austenite. Just as there is a transition region in front of a fatigue crack, there is a transition region along the austenite-martensite boundaries. However, at some point, the critical fracture criterion in the austenite is exceeded and dimples form beyond the stretched regions as noted in Fig. 6. With respect to this, it is significant that the dimples form in a direction perpendicular to the wavy slip. This means that the martensite fractures first; then fracture spreads out laterally in the austenite which is microscopically perpendicular to the macroscopic crack growth direction.

Electron fractographs were also taken from the plane stress samples. There was not nearly the amount of wavy slip that occurred in the thick samples. However, upon etching the surface with a reagent that attacked martensite, areas similar to that in Fig. 7 (a) were found in the slow growth region. No such regions were found on the shear lips of the plane stress samples and only large dimples were noted as shown in Fig. 7 (b). In all probability, the transformation is playing a predominant role during the slow crack growth process. How can this explain the fracture mode-transition? There are at least two ways in which the martensitic transformation might be connected to the fracture mode, one being related to M_D and the other to microfracture in the martensite.

With respect to M_D, if the temperature at the crack tip is locally raised above M_D, then the volume fraction of martensite produced in the plastic zone would decrease. This could occur if the crack growth rate became sufficiently rapid so that the thermal diffusivity was insufficient to carry the heat away. As the crack growth rate is directly proportional to the crosshead rate [10], perhaps this could explain the effects observed in Fig. 1. One comment is in order about alloy *B* which did not seem to exhibit a rate effect. As these specimens were tested at −196 °C, the liquid bath could change the heat-flow conditions at the crack tip as compared to room temperature tests in air. Additional tests must be run to clarify this point.

With respect to microfracture of the martensite, it was observed fractographically that the martensite fractured first. It is proposed that these microfractures form fissures in the direction of crack prolongation *. At this point, it is much easier for the crack to move laterally and connect up between fissures than to form a macroscopic shear fracture. Thus, the crack continues to propagate in a flat mode as long as the volume fraction of strain-induced martensite remains high. It is suggested that in order to accomplish this effect, that the microfracture of the martensite must be a cooperative venture between a number of plates. That is, the wavy slip region (martensite) was found to be about 15 μ in width. However, the largest strain-induced martensite plates in these materials are on the order of 2 μ in width and in general are much smaller than this. Thus, groups of martensite plates may be fracturing along a similar crystallographic plane.

This suggests that the strain-induced martensite may be lined up in one direction on a local scale. This may be possible and perhaps likely. Some evidence was obtained during the evaluation of a polished tensile sample with a width to thickness ratio of about eight [11]. During tension, a Luders' band passed about half way up the gage section. The specimen was then unloaded and it was observed that about thirty percent martensite had been produced. A micrograph taken from the strained region is shown in Fig. 8. Six measurements of the major martensitic regions indicated that they occurred at an angle of 53 °18′ to 56 °32′ with the tensile axis. The average was 54 °40′ which is nearly identical to the theoretical oblique shear angle of 54 °44′. It is also seen that there is a second set of smaller martensite 'hinges' lined up in the direction of the tensile axis. This type of martensite had been identified previously by Maksimova and Nikonorova [12] as 'bracket' martensite. Both of these, in effect, reduce the strain energy of the system and so there is an energy argument in favor of the strain-induced martensite being lined up in one

* This would qualitatively be in agreement with the delaminations observed in Fig. 2.

or perhaps two directions. Energetically, the conditions at a crack tip should result in a similar situation.

Effect of the transformation on plastic energy dissipation

Assuming that the invariant shear of the martensite transformation does take place to minimize the strain energy in the system, then one may look upon this as an energy absorbing mechanism. The following analysis treats the separate contributions of the martensite, the invariant shear and the austenite as energy absorbing media. First, consider martensite that has already been formed in front of the crack. The plastic energy absorption in this martensite would be the volume fraction that is present times the summation of strain energy density for the martensite throughout the plastic zone. Thus,

$$U_{\alpha'} = t \int_0^{2\pi} \int_0^{R_p} V_{\alpha'} W_{\alpha'} r f(\theta)\, dr d\theta \tag{2}$$

where $V_{\alpha'}$ is the volume fraction of the martensite, $W_{\alpha'}$ is the strain energy density of the martensite, t is the plate thickness, R_p is the plastic zone length, $f(\theta)$ is a shape factor and r, θ are polar coordinates. Both $V_{\alpha'}$ and $W_{\alpha'}$ are a function of plastic strain and hence a function of distance, r, away from the crack tip. It has been observed that the greater the strain, ϵ, the greater the volume percent martensite that is strain-induced [13]. Data have been obtained from magnetic field strength measurements which alloys an approximate relationship between $V_{\alpha'}$ and ϵ. As shown for two alloys in Fig. 9, this is given by

$$V_{\alpha'} \simeq 1{\cdot}2\,\epsilon^{1/2} \tag{3}$$

For large strains, the strain energy density may be approximated as $\sigma_{y\alpha}\epsilon$. Thus, equation (2) becomes

$$U_{\alpha'} = t \int_0^{2\pi} \int_0^{R_p} V_{\alpha'} \sigma_{\alpha'} \epsilon r f(\theta)\, dr d\theta \tag{4}$$

where $\sigma_{\alpha'}$ is the yield strength of the strain-induced martensite. From Hult and McClintock's strain distribution for longitudinal shear [14] the tensile analogy is taken which has been shown to adequately describe plastic strain distributions [15]. This is given by

$$\epsilon = \frac{\sigma_c}{E}\left[\frac{R_p}{r} - 1\right] \tag{5}$$

where σ_c is the yield point of the austenite-martensite mixture at the onset of plastic flow. Combining equations (3), (4) and (5) leads to

$$U_{\alpha'} = t \int_0^{2\pi} \int_0^{R_p} 1{\cdot}2\sigma_{\alpha'} \left\{ \frac{\sigma_c}{E} \left[\frac{R_p}{r} - 1 \right] \right\}^{1/2} \left\{ \frac{\sigma_c}{E} \left[\frac{R_p}{r} - 1 \right] \right\} r f(\theta)\, dr d\theta \qquad (6)$$

The shape factor was determined with the experimentally observed shape in mind. Plastic zones in these steels have been observed to be similar to the Dugdale [16] zone but somewhat fatter. Considering the total length of the zone to be R_p, the plastic strip height is usually about one-half R_p. Thus, the shape factor may be estimated approximately by assuming an ellipse with R_p for its major axis and $\frac{1}{2}R_p$ for its minor axis. Integrating $f(\theta)$ gives a shape factor of $\pi/8$. This, inserted into equation (6) and integrating from 0 to R_p gives

$$U_{\alpha'} = 0{\cdot}56\, \sigma_{\alpha'} \left(\frac{\sigma_c}{E} \right)^{3/2} R_p{}^2 t \qquad (7)$$

A similar development for the contribution of the transformation strain, ϵ_{IS}, considers the strain energy density to be $\sigma_{\alpha'}\epsilon_{IS}$. This would probably be an upper bound since stresses of $\sigma_{\alpha'}$ are not necessarily maintained at the austenite-martensite interface. Again, using the shape factor of $\pi/8$,

$$U_{IS} = \frac{\pi}{8} t \int_0^{R_p} V_{\alpha'} \sigma_{\alpha'} \epsilon_{IS}\, r\, dr \qquad (8)$$

It is noted that the contribution of the invariant shear is dependent upon the volume percent martensite, which is dependent upon the plastic strain distribution in front of the crack. Combining equations (3), (5) and (8) and integrating gives

$$U_{IS} = 0{\cdot}185\, \sigma_{\alpha'} \left(\frac{\sigma_c}{E} \right)^{1/2} \epsilon_{IS} R_p{}^2 t \qquad (9)$$

A treatment for the contribution of the austenite is identical to that of the martensite except for the volume fraction of austenite which is $1 - V_{\alpha'}$. This leads to

$$U_\gamma = 0{\cdot}196\, \frac{\sigma_\gamma \sigma_c}{E} R_p{}^2\, t - 0{\cdot}56\, \sigma_c \left(\frac{\sigma_c}{E} \right)^{3/2} R_p{}^2 t \qquad (10)$$

Using equations (7), (9) and (10) as estimates of the plastic energy dissipation, it was of interest to apply them to the experimental results.

For the 6-in wide plate of alloy B tested at –196 °C, the following parameters are appropriate:

$$\sigma_\gamma \sim \sigma_c = 258 \text{ Ksi}, \; E \simeq 30 \times 10^6 \text{psi}$$

$$\sigma_{\alpha'} \simeq 386 \text{ Ksi}, \; \epsilon_{IS} \simeq 19°; \; \epsilon_{IS} = \tan(19°) = 0{\cdot}344$$

The austenite yield strength is not actually known but since there was little yielding prior to the yield point, this is approximated as σ_c. The strength of the martensite at –196 °C was taken from some data by Chanani [17] for an almost identical composition. His material had been cold-rolled to strain-induced martensite and was subsequently tested at –196 °C. It is realized that cold-working of the martensite might raise its strength slightly above martensite strain induced during a tensile test. However, the strength of alloy B tested at –196 °C was observed to have an ultimate strength of 327 Ksi and so the 386 Ksi estimate for 100 percent martensite is probably not too unrealistic. The invariant shear of 19° is typical for the several types of martensite that might be occurring in these steels. These values in conjunction with equations (7), (9) and (10) give

Alloy B – 450
Tested at –196 °C

$$\begin{cases} U_{\alpha'} = 174\, R_p{}^2 t \text{ psi} \\ U_{IS} = 2300\, R_p{}^2 t \text{ psi} \\ U_\gamma = 314\, R_p{}^2 t \text{ psi} \end{cases}$$

$$\text{Total} = 2788\, R_p{}^2 t \text{ psi for one enclave}$$

$$U_p = 5576\, R_p{}^2 t \text{ psi for entire plate} \qquad (11)$$

All that is needed is a value for R_p. It was observed that the plastic zone was well outlined by the transformation as indicated in Fig. 3. After the fracture of the 6-in wide plate (see last line of Table 2), the plastic strip height was measured as a function of crack position. This is shown in Fig. 10 along with measured through the thickness strains. As expected, the plastic strip height and plastic strain increased with increasing crack length, i.e. increasing stress intensity. The plastic strip height was observed to be about $\frac{1}{2}R_p$. Thus, R_p was estimated from the data in Fig. 10 which allowed estimates of U_p from equation (11). These data are shown as plastic energy dissipation per unit thickness versus slow crack growth in Fig. 11. An estimate of the plastic energy dissipation rate is obtained from

$$G_p = \frac{\partial U_p}{\partial a} \cdot \frac{1}{t} \qquad (12)$$

which in this case gives 1880 lb/in toward the end of slow crack growth. This is represented by the upper triangle in Fig. 11. In terms of stress intensity,

$$K_p = [E\ G_p]^{1/2} \tag{13}$$

and 1880 lb/in represents a K value of 240 Ksi-in. This compares well with the observed value of 277 Ksi-in$^{1/2}$.

It was of interest to see if a theoretical estimate of the plastic zone size would give comparable results. The Dugdale [16] estimate was utilized as given by

$$R_p = a\left[\sec\left(\frac{\pi\sigma}{2\sigma_{ys}}\right) - 1\right] \tag{14}$$

This was modified by a Westergaard [18] finite width correction since this was shown by Gerberich and Zackay [19] to reasonably represent plastic zone estimates in wide plates. This revises equation (14) to

$$R_p = \frac{W}{\pi}\tan\left(\frac{\pi a}{W}\right)\left[\sec\left(\frac{\pi\sigma}{2\sigma_{ys}}\right) - 1\right] \tag{15}$$

Combining this with equation (11) and invoking equation (12) gives

$$G_p = 5576\left[\sec\left(\frac{\pi\sigma}{2\sigma_{ys}}\right) - 1\right]^2 \frac{2W}{\pi}\tan\left(\frac{\pi a}{W}\right)\sec^2\left(\frac{\pi a}{W}\right)\text{ psi} \tag{16}$$

For the test under discussion, the applied stress was 78·4 Ksi, the yield strength was 258 Ksi and the critical crack length was 4 in. For the 6-in wide plate, this gives a value of 1840 lb/in for G_p which may be translated into a stress intensity of 236 Ksi-in$^{1/2}$. Thus, again the estimate of K is very close to the observed value of 277 Ksi-in$^{1/2}$. It should be mentioned that to determine equation (16) it was necessary to assume that $d\sigma/da$ was zero at instability. This was essentially the case in that the increase in applied load was almost negligible toward the end of the slow crack growth process.

One other test of this proposed model was made with a 6-in wide plate specimen of the A' heat tested at room temperature. It was loaded in tension until the loading-pin hole yielded. At this point the crack had grown to 2·15 ins and the stress intensity from equation (1) was 191 Ksi-in$^{1/2}$. Just as before, the plastic energy dissipation for the various

contributions were calculated. The appropriate parameters for alloy A' tested at room temperature are:

$$\sigma_\gamma \sim \sigma_c = 201\text{ Ksi},\ E = 30 \times 10^6\text{ psi}$$

$$\sigma_{\alpha'} \simeq 290\text{ Ksi},\ \epsilon_{IS} \simeq 0{\cdot}344$$

These values in equations (7), (9) and (10) give

Alloy A' – 450
Tested at 20 °C

$$\begin{cases} U_{\alpha'} = 90\ R_p^2 t\text{ psi} \\ U_{IS} = 1590\ R_p^2 t\text{ psi} \\ U_\gamma = 200\ R_p^2 t\text{ psi} \end{cases}$$

Total = $1880\ R_p^2 t$ psi for one enclave

$U_p = 3660\ R_p^2 t$ psi for entire plate (17)

Using this result, a derivation for G_p similar to equation (16) gives a value of 1620 lb/in for G_p and a stress intensity of 221 Ksi-in which compares reasonably well with the 191 Ksi-in$^{1/2}$ value observed.

One comment is in order about the various contributions of the plastic energy dissipation. If the invariant shear contribution is about 5 times as great as what is normally obtained in high strength steels, why is the toughness not $\sqrt{(5)}$ times as great? The plastic zone in these steels is long but narrower than in many materials having some degree of work hardening. Thus, the shape factor of $\pi/8$ for the materials of this investigation compares to values nearer $\pi/2$ for other steels. Consequently, even though the plastic energy dissipation is greater per unit volume of material involved, the contributing volume is smaller. One might say that the strain-induced transformation allows more efficient use of a narrower plastic zone. This may have some advantage under plane strain conditions where the plastic zone size is limited by geometrical considerations, such as plate thickness. Perhaps this is why no toughness transition was detected in the room temperature data of alloy A' – 450, even with one-inch thick samples.

Conclusions

1. The toughness of steel undergoing a strain-induced transformation at the crack tip is very good.
2. The transformation interacts with the crack tip to allow propagation in a macroscopic flat mode rather than a macroscopic shear mode.
3. Fractographic observations indicate that the microscopic fracture process is a ductile one. Initial fissures in the direction of crack propagation form by wavy glide in strain-induced martensite followed by lateral tearing of the austenite between fissures.

Fig. 4. Typical fractograph taken from a thick sample of B-450 material tested at −196°C.

Fig. 5. Fractograph showing slow crack growth emanating from fatigue crack.

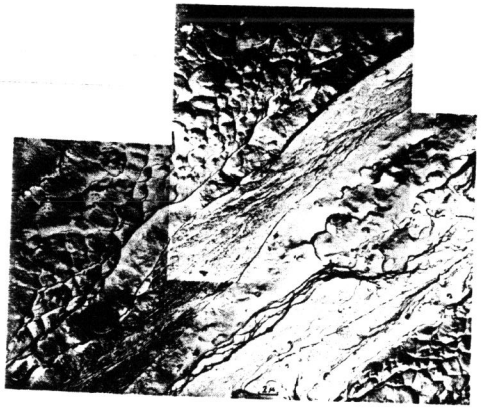

Fig. 6. Wavy glide, stretched regions and dimpled rupture on fracture surface of austenite-martensite mixture.

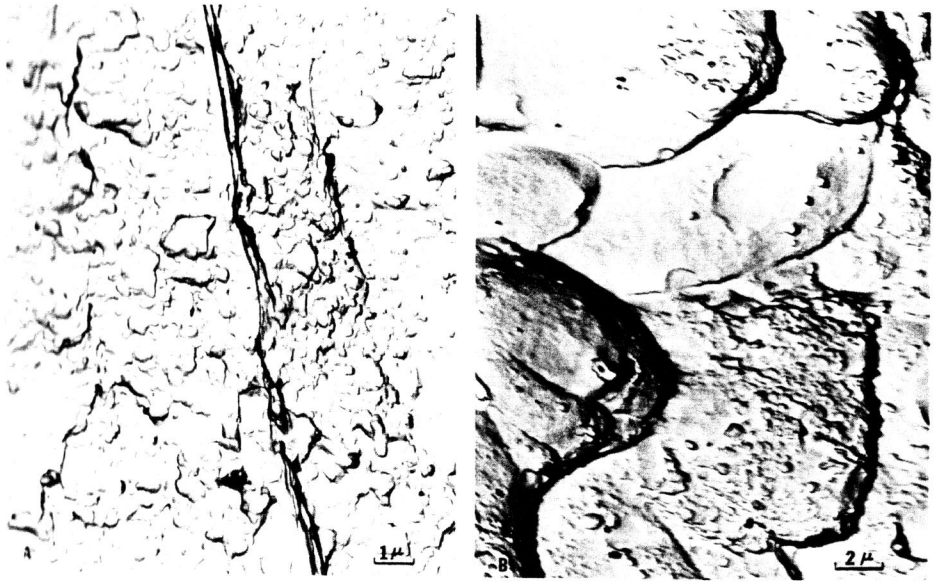

Fig. 7. Fractographs taken from the flat (a) and shear (b) regions of a thin sample of B-450 material tested at −196°C.

Fig. 8. Brackett martensite forming on tensile and shear axes of tensile specimen.

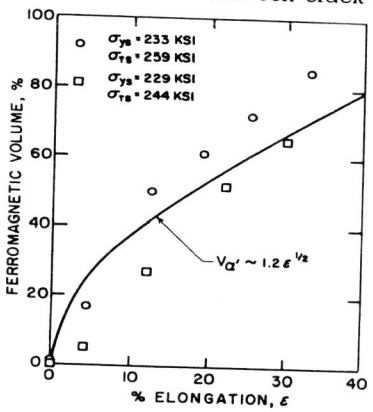

Fig. 9. Relationship between strain and volume fraction of strain-induced martensite.

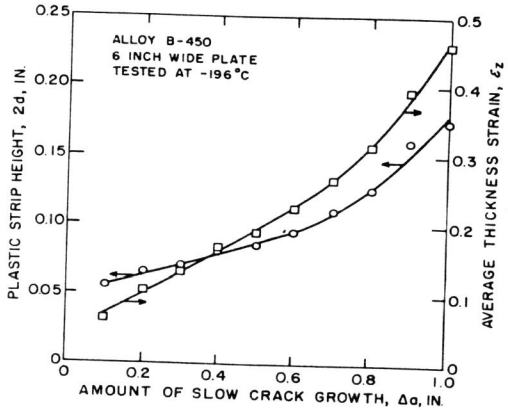

Fig. 10. Measured plastic strip height and thickness strains as a function of crack length.

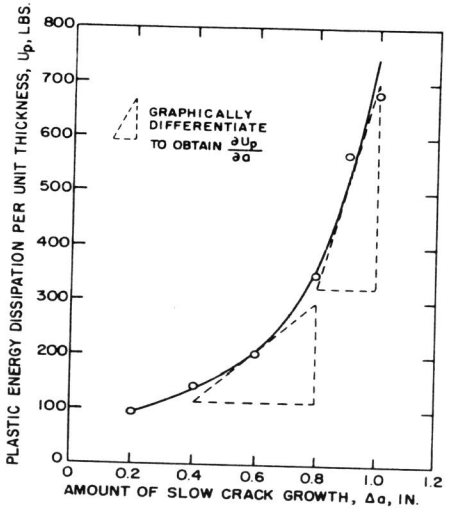

Fig. 11. Estimate of plastic energy dissipation as a function of crack length.

Table 1. Uniaxial tensile data

Material and treatment	*Test condition*	*Yield strength,*[a] *Ksi*	*Ultimate strength,*[a] *Ksi*	*Elongation*[a] *(1 in.), %*
A-250	RT – 0·001 in/sec.	234·5	235·5	31·5
A-250	–196 °C – 0·001 in/sec.	256·2	294·0	13·0
A'-450	RT – 0·001 in/sec.	201·0	239·5	35·6
A'-450	–73 °C – 0·001 in/sec.	185·0	284·0	21·0
A'-450	–196 °C – 0·001 in/sec.	195·2	366·5	18·0
B-450	RT – 0·001 in/sec.	181·7	196·2	9·6[b]
B-450	–73 °C – 0·001 in/sec.	211·7	222·0	46·6
B-450	–196 °C – 0·001 in/sec.	258·0	326·9	38·9

(a) Average of duplicate or more tests (b) Almost no strain-induced martensite

Table 2. Plane stress fracture data

Material and treatment	*Test condition*	*Thickness in*	*Width in*	*Applied stress, Ksi*	*Initial crack, in*	*Critical crack, in*	*Stress intensity, Ksi-in*$^{1/2}$
A-250[a]	RT – 0·0002 in/sec.	0·079	2·72	34·9	1·06	None	(b)
A-250[a]	RT – 0·002 in /sec.	0·081	2·71	41·1	0·97	1·47	289
A-250[a]	RT – 0·02 in/sec.	0·082	2·72	36·9	1·01	1·45	250
A-250[a]	RT – 0·2 in/sec.	0·083	2·75	33·5	1·04	1·37	199
A'-450[c]	RT – 0·0001 in/sec.	0·0825	6·00	96·0	2·05	2·15[d]	1 1[d]
B-450[c]	–196 °C – 0·0005 in/sec.	0·080	5.00	71·0	1·83	3·47	244
B-450[c]	–196 °C – 0·005 in/sec.	0·080	5·00	80·0	1·75	3·83	314
B-450[c]	–196 °C – 0·05 in/sec.	0·073	6·00	78·4	1·75	4·00	277

(a) Single-edge notch specimen (c) Center-notch specimen
(b) Crack slowly teared giving no instability (d) Pin-loading hole failed, specimen unloaded.

Table 3. Plane strain fracture data

Material and treatment	Test condition	Thickness, in	Width, in	Initial crack in	Load at linear deviation	Maximum load	Stress intensity Ksi-in$^{1/2}$ (a)	(b)	(c)
A'-450	−196 °C − 0·005 in/sec.	0·49	2·12	1·17	6,300	6,460	108	111	–
A'-450	−196 °C − 0·001 in/sec.	1·06	2·38	1·25	9,900	12,600	67·5	86·0	106
A'-450	RT − 0·001 in/sec.	0·495	2·14	0·71	8,500	14,750	81·3	141	206
A'-450	RT − 0·001 in/sec.	0·493	1·38	0·57	6,750	10,500	83·5	130	–
A'-450	RT − 0·001 in/sec.	0·968	2·37	1·35	8,700	15,150	74·6	130	173
A'-450	RT − 0·001 in/sec.	0·877	2·38	1·31	10,200	15,100	90·6	134	177
B-450	−196 °C − 0·0005 in/sec.	0·48	2·11	0·60	14,700	15,800	133·0	143·0	–
B-450	−196 °C − 0·0005 in/sec.	0·49	2·18	0·65	13,500	16,050	121·0	143·5	–
B-450	RT − 0·0005 in/sec.	0·49	2·10	0·64	16,500	23,000	153	213	–
B-450	RT − 0·0005 in/sec.	0·48	2·19	0·56	18,000	19,800	153	168[(d)]	–

(a) At linear deviation
(b) At maximum load and initial crack
(c) At maximum load and crack length at maximum load
(d) Specimen unloaded.